ACADEMIA ROMÂNĂ
Şcoala de Studii Avansate a Academiei Române
Institutul de Chimie Macromoleculară „Petru Poni” din Iași

COMPOSITE MEMBRANES FOR FUEL CELLS

Summary of doctoral thesis

SCIENTIFIC COORDINATOR:

Dr. ing. Valeria Harabagiu

Ph.D. STUDENT:

Laurențiu Baltag

2025

CUPRINS

INTRODUCTION

The growing global interest in alternative and sustainable energy sources has emerged as a response to the depletion of fossil fuel reserves, the environmental impact of pollution, and the effects of climate change. Proton exchange membrane fuel cells (PEMFC) are considered a promising solution for clean energy generation due to their high efficiency and near-zero emissions during operation.

The subject of this thesis, Composite Membranes for Fuel Cells, addresses an important challenge: the development of clean and sustainable energy sources. The increasing worldwide interest in alternative and sustainable energy technologies is driven by the exhaustion of fossil resources, environmental pollution, and climate change. Proton exchange membrane fuel cells represent a promising technology for clean energy production, being characterized by high efficiency and negligible emissions during operation.

The thesis is structured into two parts. Part I, consisting of Chapter 1, presents a literature review and provides an analysis of studies focused on proton exchange membrane fuel cells. Part II, entitled Original Contributions, comprises Chapters 2–5.

Chapter 2 focuses on the experimental aspects of the work, including the materials and methods used for the preparation of intermediates and composite membranes, as well as the techniques employed for process monitoring and product characterization.

Chapter 3 presents details regarding the synthesis of intermediates (fillers - ferrites, perovskites, and core@shell nanoparticles) and the polymer matrix, sulfonated poly(ether ether ketone) (SPEEK). It also describes their structures and physicochemical properties as influenced by the synthesis conditions.

Chapter 4 begins with a subsection presenting preliminary results obtained from investigating the influence of the chemical nature and properties of the fillers (synthesized within this work, together with commercially available titanium dioxide) on the properties of the composite membranes. The results enabled the selection of praseodymium-doped ferrites as the most suitable fillers for the preparation of polyelectrolyte membranes. The second and third subsections of this chapter focus on the optimization of the composite membranes through the evaluation of the effect of ferrite content on proton conductivity.

In this thesis, six metal oxides **($CoFe_2O_4$, $ZnFe_{1,96}Pr_{0,04}O_4$, $NiFe_{1,96}Pr_{0,04}O_4$, $Zn_{0,5}Ni_{0,5}Fe_{1,96}Pr_{0,04}O_4$, $CaMnO_3$, Gd_2MnFeO_6)** were synthesized using the sol–gel auto-combustion method, together with two types of core@shell nanoparticles

($ZnFe_{1,96}Pr_{0,04}O_4@TiO_2$, $NiFe_{1,96}Pr_{0,04}O_4@TiO_2$). Sulfonated poly(ether ether ketone) with a high degree of sulfonation was successfully obtained within a short reaction time using a novel procedure recently reported in the literature.

New SPEEK-based composite membranes were prepared using the synthesized metal oxides as fillers, and their properties were evaluated for potential application in PEMFC. The effect of the filler type on the properties of the composite membranes, including proton conductivity, was systematically investigated.

For the **SPEEK/$ZnFe_{1,96}Pr_{0,04}O_4$, SPEEK/$NiFe_{1,96}Pr_{0,04}O_4$** systems (the membranes exhibiting the best overall performance), the optimal filler concentrations were established.

Composite membranes exhibiting proton conductivity and overall performance comparable to, or higher than, those of the commercial membrane Nafion117, used as a reference and tested under identical conditions, were successfully obtained.

The proton conductivity values determined by the indirect method of dielectric spectroscopy will be further validated through testing of the optimized membranes in hydrogen fuel cells.

CHAPTER 3. SYNTHESIS AND CHARACTERIZATION OF INTERMEDIATES

3.1. Introduction

The intermediates used in this study for the fabrication of proton exchange composite membranes consist of oxide fillers (ferrites, perovskites, titanium dioxide, and ferrite@TiO_2 core@shell nanoparticles) and the polymer matrix, sulfonated poly(ether ether ketone) (SPEEK). This chapter provides a detailed description of their synthesis and properties, with the objective of selecting the most suitable material combinations for the development of high-performance proton exchange membranes (PEM).

3.2. Fillers

Given their relatively hydrophilic character [152] and their ability to scavenge free radicals [153], we decided to investigate the feasibility of SPEEK/ferrite composites as proton exchange membranes (PEM), with particular emphasis on the effects of filler chemical structure and filler loading on the physical and chemical properties of the resulting membranes, including proton conductivity. Besides spinel ferrites, perovskite-type oxides and core–shell nanoparticles composed of spinel ferrites coated with titanium dioxide were also synthesized and evaluated [115,154].

3.2.1. Synthesis of spinel ferrites and perovskites by sol-gel auto-combustion method

Four ferrites (cobalt-, nickel-, and/or zinc-based, doped with praseodymium), as well as two perovskite samples (a simple calcium, manganese, perovskite and a double gadolinium, manganese and iron perovskite), were prepared by the sol-gel auto-combustion method (Figure 3.1), with modifications based on established procedures reported in the literature [92,155,156].

For all samples, the cation precursors were hydrated metal nitrates, which are water-soluble, except for the double perovskite, whose synthesis started from gadolinium oxide and required a preliminary dissolution step in nitric acid. As chelating/combustion agents, anthranilic acid, urea, or a citric acid/ethylene glycol mixture were used, selected in order to obtain nanoparticles with small particle sizes following the gelation and auto-combustion processes.

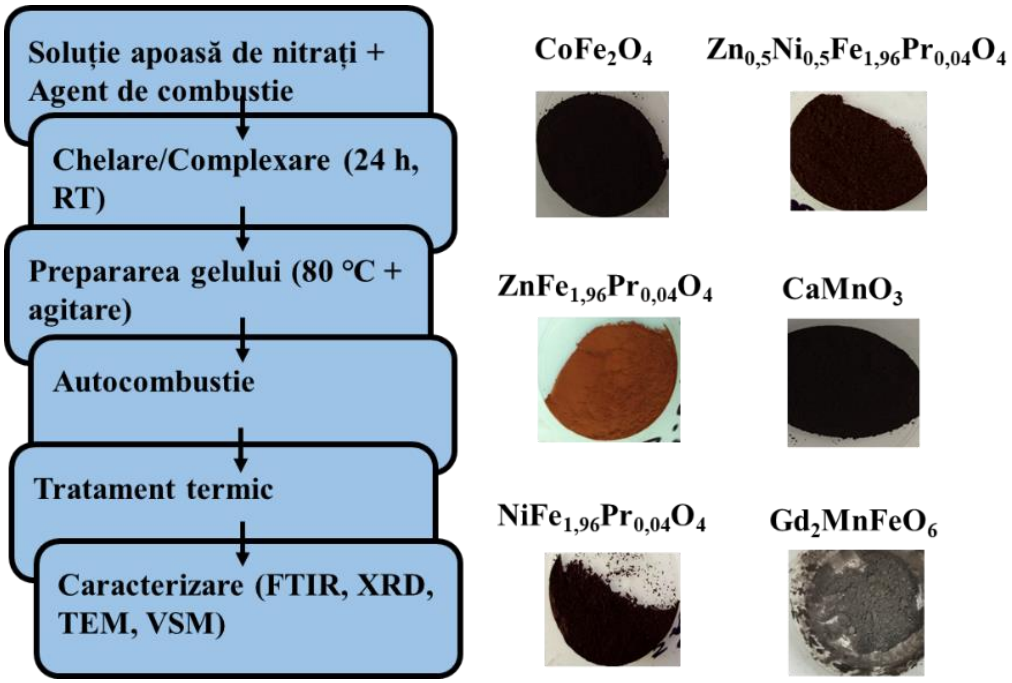

Figure 3.1. Schematic representation of the synthesis process of perovskites and spinel ferrites

3.2.2. Characterization of spinel ferrite and perovskites

The fillers influence both the membrane fabrication process and the properties of the resulting membranes through their chemical structure, morphology, particle size, and physicochemical characteristics. The chemical structures of the ferrites and perovskites were characterized by infrared spectroscopy (FTIR), the crystalline structures were investigated by wide angle X-ray diffraction (XRD). Particle size and morphology were examined using transmission electron microscopy (TEM), while magnetic properties were evaluated by vibrating sample magnetometry (VSM).

The FTIR spectrum of cobalt ferrite, recorded for the sample thermally treated at 900 °C, exhibits absorption bands in the 600-400 cm^{-1} region, which are characteristic of metal-oxygen bond vibrations, for the tetrahedral sites (Fe-O at 582 cm^{-1}) and octahedral sites (475 cm^{-1} for Fe–O and 412 cm^{-1} for Co-O). These results confirm the formation of an inverse spinel structure.

The FTIR spectra of zinc ferrite, nickel ferrite, and mixed zinc–nickel ferrite, all doped with praseodymium and thermally treated at 700 °C, also confirm the formation of the spinel structure. For all three doped ferrites, in addition to the characteristic metal-oxygen absorption bands below 600 cm^{-1}, vibrations assigned to Zn-O and/or Ni-O bonds (cations occupying tetrahedral sites) appear at higher wavenumbers, whereas Fe-O vibrations (cations occupying octahedral sites) are observed at lower wavenumbers. The relatively

intense band located at approximately 1620 cm^{-1}, characteristic of water adsorbed from the atmosphere during sample handling, indicates their hydrophilic nature.

In the case of $CaMnO_3$, three absorption bands can be observed at approximately 600 cm^{-1} and 578 cm^{-1}, corresponding to metal–oxygen stretching vibrations, and at 460 cm^{-1}, which is characteristic of the O-metal-O bending vibration. Similar absorption bands associated with metal–oxygen bonds are also present in the spectrum of Gd_2MnFeO_6; however, these bands are broader (770-490 cm^{-1} and 480-400 cm^{-1}).

The formation of the crystalline structures of the fillers was confirmed by correlating the diffraction peaks observed in the X-ray diffraction patterns with reference data or the data reported in the literature (Figures 3.6–3.8).

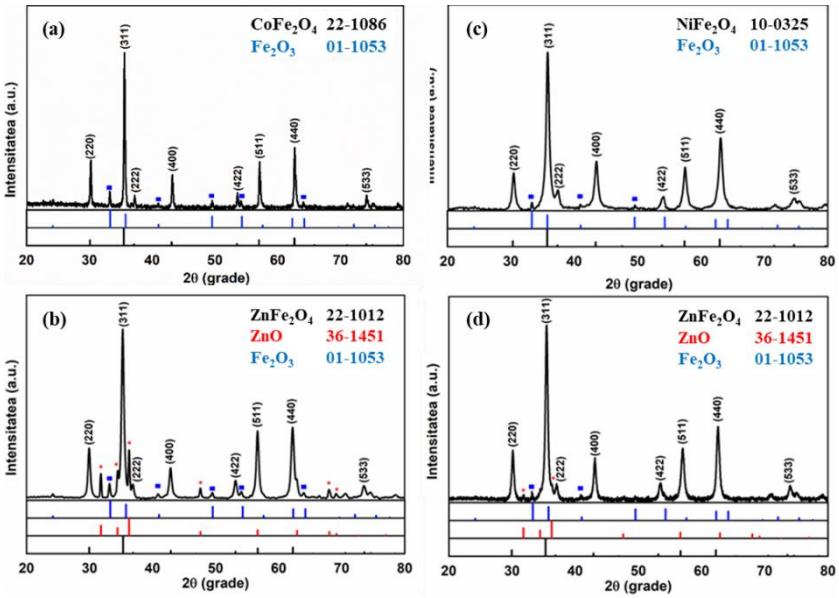

Figure 3.6. X-ray diffraction patterns of the synthesized ferrites and the reference data used for the identification of the crystalline phase: (a) $CoFe_2O_4$; (b) $ZnFe_{1,96}Pr_{0,04}O_4$; (c) $NiFe_{1,96}Pr_{0,04}O_4$; (d) $Zn_{0,5}Ni_{0,5}Fe_{1,96}Pr_{0,04}O_4$

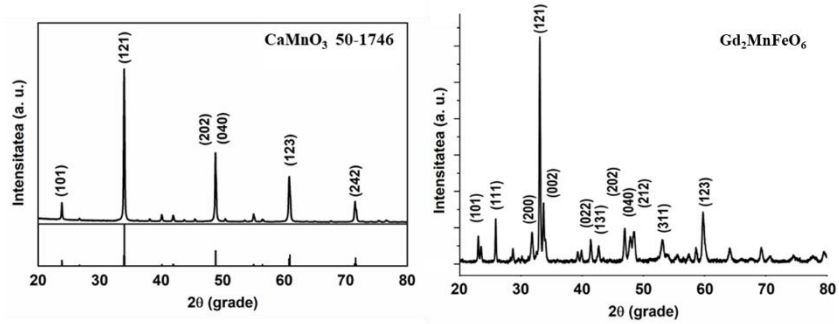

Figure 3.7. X-ray diffraction patterns of the perovskites: $CaMnO_3$ (together with the JCPDS reference card used for phase identification) and Gd_2MnFeO_6, with the diffraction planes assigned according to literature data [156]

The characteristic peak intensities of the two distinct crystalline structures are higher for the titanium dioxide phases than for the ferrite phases, owing to the TiO_2/ferrite mass ratio of 4:1. Furthermore, it can be observed that the intensities of the newly emerged peaks associated with the anatase and rutile phases differ between the two samples, indicating different anatase and rutile phase ratios. This ratio can be determined from the X-ray diffraction patterns using the Spurr–Myers method [164]. Applying this method yielded the following phase compositions: for $ZnFe_{1,96}Pr_{0,04}O_4@TiO_2$, 16.3% rutile and 83.7% anatase; and for $NiFe_{1,96}Pr_{0,04}O_4@TiO_2$, 42.6% rutile and 57.4% anatase. The lower rutile content observed in the $ZnFe_{1,96}Pr_{0,04}O_4@TiO_2$ sample may be attributed to the inhibitory effect of zinc on the anatase-to-rutile phase transformation at the calcination temperature employed (500 °C), in agreement with results reported by other authors [166,167].

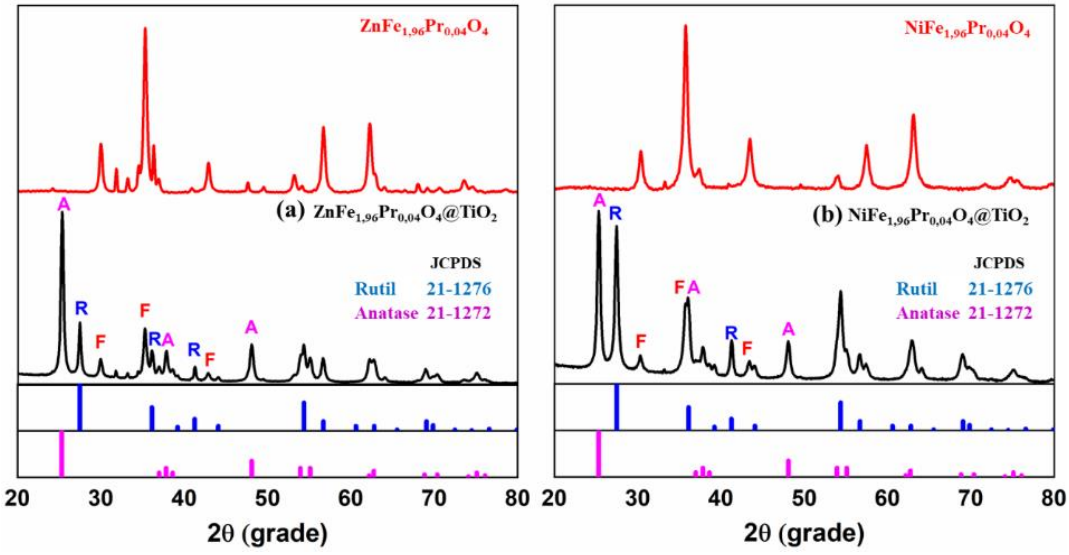

Figure 3.8. X-ray diffraction patterns of the core–shell nanoparticles: (a) $ZnFe_{1,96}Pr_{0,04}O_4@TiO_2$, (b) $NiFe_{1,96}Pr_{0,04}O_4@TiO_2$

Crystallite size and the particle size for the fillers are represented in Table 3.2. The crystallite size was calculated using Debye-Scherrer equation.

Table 3.2. Average crystallite and particle size of the fillers

Sample	**Crystallie size* (nm)**	**Particle size** nm**
$CoFe_2O_4$	42	81
$ZnFe_{1,96}Pr_{0,04}O_4$	21	23
$NiFe_{1,96}Pr_{0,04}O_4$	16	23
$Zn_{0,5}Ni_{0,5}Fe_{1,96}Pr_{0,04}O_4$	21	29
$CaMnO_3$	44	220
Gd_2MnFeO_6	47	220
$ZnFe_{1,96}Pr_{0,04}O_4@TiO_2$	-	38

*** for the peak with the highest intensity (from XRD);**
**** from TEM**

The following magnetic parameters were evaluated from the hysteresis curves: coercivity (H_C), intrinsic coercivity (H_{CI}), saturation magnetization (M_S), and remanent magnetization (B_r). Among the synthesized ferrites, cobalt ferrite and praseodymium doped mixed zinc-nickel ferrite exhibited the highest saturation magnetization values. This results in a stronger tendency toward particle agglomeration and leads to poor and non-uniform dispersion within the polymer matrix.

Table 3.3. Magnetic properties of fillers

Sample	Coercivity (Oe)	Intrinsic coercivity (Oe)	Remanance (emu/g)	Magnetization (emu/g)
$CoFe_2O4$	10.7	988	30	69
$ZnFe_{1,96}Pr_{0,04}O_4$	0,005	13,7	0,02	4,7
$NiFe_{1,96}Pr_{0,04}O_4$	1,9	135,1	5	31,4
$Zn_{0,5}Ni_{0,5}Fe_{1,96}Pr_{0,04}O_4$	3,1	56,8	5,6	62
$CaMnO_3$	0.02	53	0.002	0.6
Gd_2MnFeO_6	0,8	88	0.06	3.2

Praseodymium doped zinc ferrite exhibits low coercivity and remanence values, as well as low saturation magnetization compared to the other synthesized ferrites, with magnetization values similar with those reported in the literature [168].

From the obtained magnetic parameters, it can be observed that a stronger magnetic field is required to reduce the magnetic field to zero (coercivity) for the mixed zinc-nickel ferrite than for nickel ferrite. However, a higher magnetic field is needed to completely demagnetize the nickel ferrite (intrinsic coercivity) compared with the mixed zinc-nickel ferrite. Nickel ferrite and the mixed ferrite exhibit similar remanent magnetization values, whereas the mixed ferrite displays a saturation magnetization approximately twice as high.

From the hysteresis curves of the perovskites, we can observe a paramagnetic response for the calcium-manganese perovskite and a combined paramagnetic-ferromagnetic behavior for the gadolinium-manganese-iron double perovskite [156].

3.3. Polymeric matrix - sulfonated poly(ether ether ketone) (SPEEK)

Poly(ether ether ketone) (PEEK) is a semi-crystalline, hydrophobic, high-performance thermoplastic polymer. Due to its 1,4-substituted aromatic structure and the extensive conjugation along the polymer backbone, PEEK exhibits excellent thermal, mechanical, and chemical resistance. However, because it lacks proton conductivity and is inherently hydrophobic, PEEK is not suitable for direct use as a polyelectrolyte in proton exchange membrane fuel cells (PEMFC). Consequently, sulfonation of PEEK is required (Figure 2.3). Sulfonation of PEEK is an electrophilic substitution reaction in which a proton on the aromatic ring is replaced by a sulfonic acid group (-SO_3H). The introduction of sulfonic acid groups modifies the polymer properties, imparting the characteristics necessary for its application as a proton exchange membrane (PEM) [15].

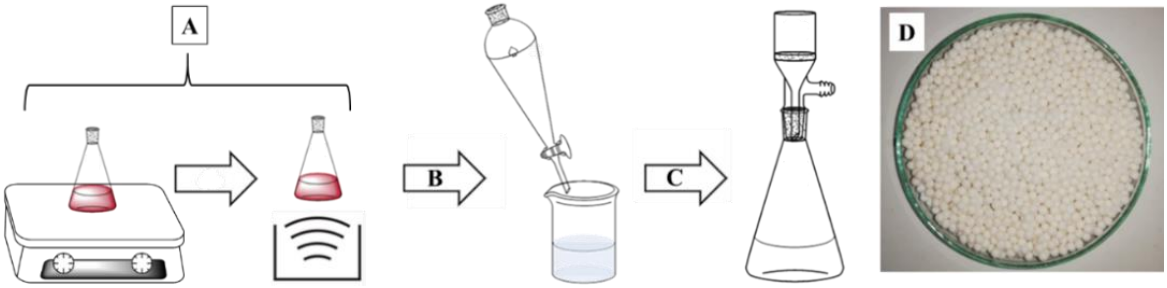

igure 2.3. General schematic representation of the PEEK sulfonation process: A-sulfonation (50 °C, 90 min) and ultrasound (60 °C, varied time); B-precipitation; C-washing; D-SPEEK spheres

In this work, the sulfonation of PEEK was carried out using concentrated sulfuric acid [169,170], with the application of ultrasonic irradiation significantly reduced the synthesis time. Sulfonated poly(ether ether ketone) (SPEEK) samples with different degrees of sulfonation were prepared by varying the reaction conditions, including temperature, heating time, and sulfonation time under ultrasonic treatment (Table 3.5).

The structure of the sulfonated polymer was confirmed by FTIR and ^{1}H-NMR analyses. The FTIR spectra of the PEEK and the sulfonated polymer (SPEEK) (Figure 3.15) were recorded using the ATR module, and the assignment of the absorption bands was performed according to literature data [128].

A comparison between PEEK and SPEEK spectra reveals an increased number of absorption bands in the 650–924 cm^{-1} region for SPEEK, from the appearance of C–S bond vibrations in addition to the C-H vibrations of the aromatic rings. Significant changes are

also observed in the 1011–1220 cm^{-1} spectral region, where the C-S, S-O, and O=S=O vibrations overlap with the characteristic C-O-C bands.

The variation of the degree of sulfonation (DS) of SPEEK as a function of ultrasonication time was monitored by NMR spectroscopy. The ^{1}H-NMR spectra allow the identification of sulfonated structural units because the proton attached to the aromatic ring substituted with a sulfonic acid group and bonded to two ether linkages, located in the ortho position relative to the sulfonic acid group, exhibits a characteristic chemical shift at approximately 7.5 ppm. This signal is distinct from those of all other hydrogen atoms present in the SPEEK structure (Figure 3.16).

Table 3.5. The variation of the degree of sulfonation of SPEEK from ^{1}H-NMR

Sample	#1	#2	#3	#4	#5	#6
Reaction condition						
*Ultrasonication time 60 ℃ (min)**	(-)	(-)	15	30	45	60
*60 ℃ (min)**	(-)	90	(-)	(-)	(-)	(-)
Degree of sulfonation (%)	39	67	61	74	83	89

* (-) samples without ultrasonication, respectively without heating at 65 ℃

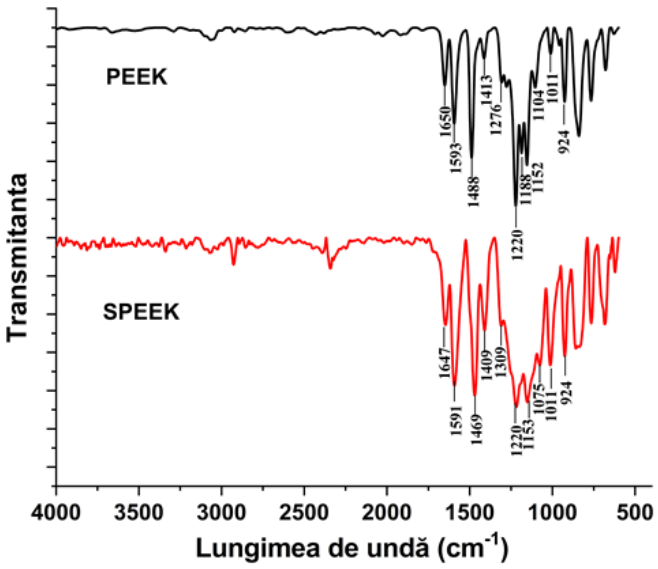

Figure 3.15. FTIR-ATR spectra of PEEK and SPEEK

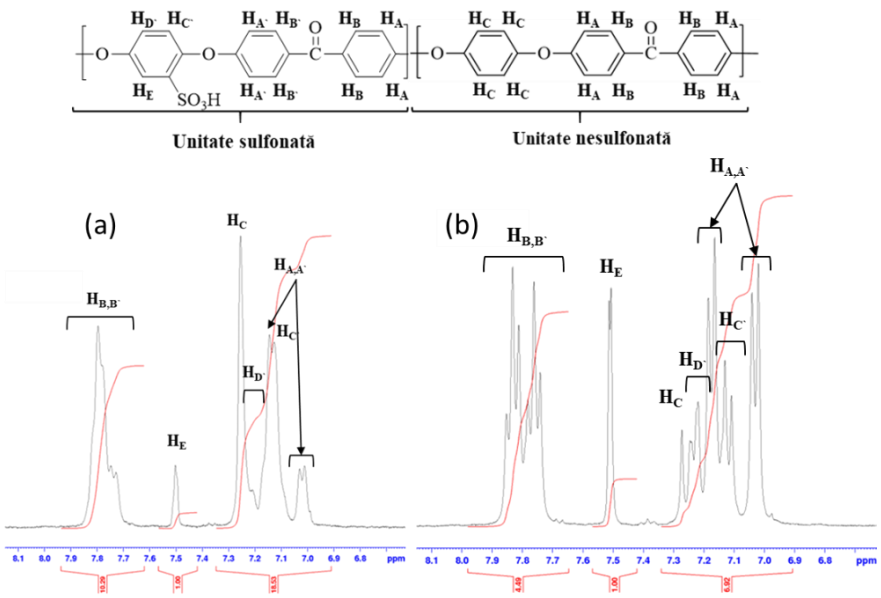

Figure 3.16. ^{1}H-RMN spectra of SPEEK sample #2

The thermal degradation curves of PEEK and the sulfonated polymer are presented in Figure 3.20. As can be observed, SPEEK exhibits two additional degradation events compared to unmodified PEEK. The first mass loss, occurring at approximately 65 °C, is attributed to the evaporation of water absorbed from the atmosphere as a result of the increased hydrophilicity imparted by the introduction of sulfonic acid groups (-SO_3H). The second mass loss occurs at temperatures above 200 °C, with a maximum degradation rate at 273 °C, and is associated with the decomposition and elimination of the sulfonic acid groups. The final degradation stage of SPEEK takes place over a broader temperature range and at lower temperatures (440-670 °C) than that of the unmodified PEEK. The residual mass at 670 °C was found to be 49% for PEEK and 42% for SPEEK.

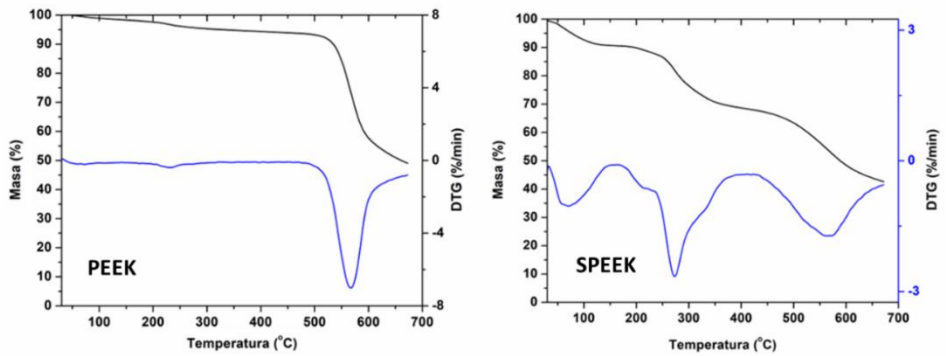

Figure 3.19. TG/DTG curves for SPEEK and PEEK

3.4. Conclusions

Metal oxides belonging to the ferrite family (**$CoFe_2O_4$**, **$ZnFe_{1,96}Pr_{0,04}O_4$**, **$NiFe_{1,96}Pr_{0,04}O_4$** and **$Zn_{0,5}Ni_{0,5}Fe_{1,96}Pr_{0,04}O_4$**) and the perovskite family (**$CaMnO_3$** and **Gd_2MnFeO_6**) were synthesized using the sol–gel auto-combustion method. The resulting materials were obtained as nanoparticles, which could be dispersed within the polymer matrix under ultrasonic treatment, and exhibited morphologies, degrees of crystallinity, and magnetic properties dependent on their chemical composition and structure. The synthesized praseodymium doped zinc ferrite and nickel ferrite exhibited the smallest particle sizes and were subsequently converted into core@shell nanoparticles through the sol-gel polycondensation of titanium tetraisopropoxide in the presence of the ferrite particles, followed by removal of the chelating agent by thermal treatment (combustion).

The polymer matrix was prepared by sulfonation of PEEK with concentrated sulfuric acid under ultrasonic irradiation. This newly proposed method proved to be more efficient by significantly reducing the duration of the sulfonation step while allowing precise control of the degree of sulfonation (39-89%%) through variation of the ultrasonication time (0-60 min). The solubility of the resulting SPEEK matrix in DMSO, required for membrane fabrication, and in water, where the membranes must remain stable under PEMFC operating conditions (approximately 80 °C) without dissolving or exhibiting excessive swelling, was strongly dependent on the degree of sulfonation. Based on these requirements, the SPEEK sample with a degree of sulfonation of 61% was identified as the most suitable and was selected as the polymer matrix for the preparation of all composite membranes.

CHAPTER 4. SPEEK/OXIDE MATERIALS COMPOSITE MEMBRANES

4.1. Introduction

To obtain proton exchange membranes with properties optimized for application in PEMFC, various preparation and modification strategies have been reported in the literature, including the incorporation of fillers, membrane crosslinking or blending with other polymers. In general, the role of fillers is to enhance the thermal, mechanical, and/or chemical stability of the membranes. At the same time, filler particles become interposed between the polymer chains of the matrix, increasing water uptake and facilitating proton transport through the interconnected ionic channels formed within SPEEK polyelectrolyte membranes (morphologies similar to those of PFSA based membranes) [41,121,179] (Figure 4.1) which can result in a increase of the proton conductivity.

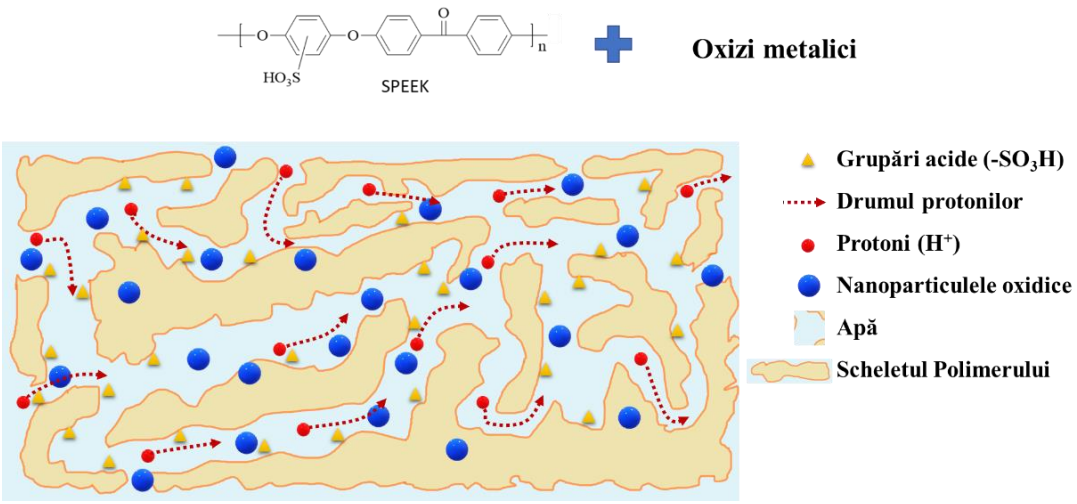

Figure 4.1. Proton transport in SPEEK/oxide nanoparticle composite membranes

This chapter addresses two main objectives. The first objective is to investigate the influence of the chemical structure of the filler material (at a constant filler loading) on the properties of the composite membranes and to identify the samples exhibiting the most favorable characteristics in terms of filler dispersibility within the polymer matrix, membrane homogeneity, and proton conductivity. The second objective is to evaluate the effect of filler content on the proton conducting performance of the membranes.

4.2. Influence of the chemical structure of fillers on membrane properties

Composite membranes based on SPEEK polymer matrix and various fillers from ferrites ($CoFe_2O_4$, $ZnFe_{1,96}Pr_{0,04}O_4$, $NiFe_{1,96}Pr_{0,04}O_4$, $Zn_{o,5}Ni_{0,5}Fe_{1,96}Pr_{0,04}O_4$) and perovskites ($CaMnO_3$, Gd_2MnFeO_6) were prepared. Seven composite membranes containing 5% filler (SPEEK/Ti5, SPEEK/Co5, SPEEK/Zn5, SPEEK/Ni5, SPEEK/ZnNi5, SPEEK/Ca5, and SPEEK/Gd5) were prepared, together with a filler-free SPEEK membrane used as a reference. A membrane containing titanium dioxide was also included for comparison purposes. Several membrane properties were investigated in order to identify the most suitable SPEEK-filler combination. These included membrane morphology, water sorption capacity, chemical stability, mechanical properties, and dielectric behavior.

Under normal circumstances, good compatibility between the oxide fillers and the SPEEK matrix is expected. This compatibility is ensured, on the one hand, by the small particle size of the fillers (Table 3.3: 23-29 nm for the ferrites and approximately 220 nm for the perovskites) and, on the other hand, by surface interactions between the oxide nanoparticles and the sulfonic acid groups of the polymer matrix. These interactions may occur through hydrogen bonding, either directly or mediated by water molecules, as well as through ionic interactions.

Among the composite membranes, those containing cobalt ferrite (SPEEK/Co5) and praseodymium doped mixed zinc-nickel ferrite (SPEEK/ZnNi5) exhibited a non-uniform dispersion of the filler in the SPEEK matrix. The aggregation of cobalt ferrite and mixed zinc-nickel ferrite particles in the membranes can be attributed to their relatively high magnetic properties. As a result, these two oxide fillers were found to be unsuitable for PEM applications, owing to their negative impact on membrane morphology and, consequently, on the overall membrane properties.

Water plays an essential role in proton transport through the membrane; therefore, water management in PEMFC is a key factor for the proper operation of the fuel cell [41]. For all membranes, water uptake occurred almost instantaneously, with substantial absorption observed in the first 5 minutes of contact. The maximum water sorption capacity did not vary significantly with the nature of the filler. Nevertheless, the lowest values were observed for the membrane containing calcium perovskite (SPEEK/Ca5: 24.0%) and for the pristine membrane (SPEEK: 25.3%), whereas the highest value was recorded for the

membrane containing titanium dioxide (SPEEK/Ti5: 26.8%). This behavior may be attributed to the hydrophilic nature of titanium dioxide as a filler material [179].

The environment within a fuel cell during operation is acidic due to the presence of protons. The stability of the prepared membranes under acidic conditions was evaluated using a sulfuric acid solution (H_2SO_4, pH=3). All composite membranes exhibited lower chemical stability in the acidic medium than the pristine membrane, with mass losses ranging from 10.7% to 13.8%. In addition, the fuel cell environment is oxidative, as the presence of oxygen and catalysts promotes the formation of reactive oxidative species. To assess membrane stability under oxidative conditions, the membranes were immersed in Fenton's reagent. Only minor differences were observed among the samples, with the exception of the membrane containing the gadolinium–manganese–iron double perovskite, which exhibited the highest mass loss (16.6% after 24 h). A slight stabilizing effect of the praseodymium-doped zinc ferrite nanoparticles on the polymer matrix was observed. The SPEEK/Zn5 membrane showed a mass loss after 24 h that was approximately 2% lower than that of the pristine SPEEK membrane. Although immersion in Fenton's reagent did not result in noticeable changes in membrane shape or appearance, all membranes became slightly brittle after 24 h of exposure. This effect was more pronounced for the SPEEK/Gd5 membrane, suggesting a possible catalytic effect of iron and, potentially, gadolinium ions on the activation of oxidative degradation processes.

The thermal degradation curves of the analyzed membranes reveal three distinct weight loss stages, occurring over relatively similar temperature ranges for all samples. The first stage, with a maximum at approximately 80 °C, is associated with dehydration, corresponding to the removal of physically absorbed water. The second stage occurs from approximately 150 °C to above 340 °C and is attributed to the evaporation of residual DMSO trapped within the membrane, as well as to the elimination of acidic groups (the degradation of the sulfonic acid functionalities ($-SO_3H$) of the polymer). The third and final stage, characterized by a maximum around 550 °C, is assigned to the thermal decomposition of the polymer backbone.

The resistance of membranes to mechanical stress is another important factor determining their suitability for fuel cell applications. To evaluate the mechanical properties of the prepared membranes, tensile stress-strain curves were recorded and are presented in Figure 4.7. All samples exhibited an initial elastic deformation region, with elongation at break values ranging between 5 and 7%, followed by a plastic deformation region. The incorporation of fillers reduced the ability of the membranes to undergo plastic deformation.

The most pronounced decrease was observed for the membranes containing perovskite fillers. These materials did not exhibit optimal compatibility with the SPEEK matrix, as evidenced by their migration toward the membrane surface, which adversely affected the mechanical integrity of the membranes. A significant reduction in plastic deformation was also observed for the membrane containing nickel ferrite. This behavior is most likely related to the magnetic properties of the ferrite particles, which promote agglomeration.

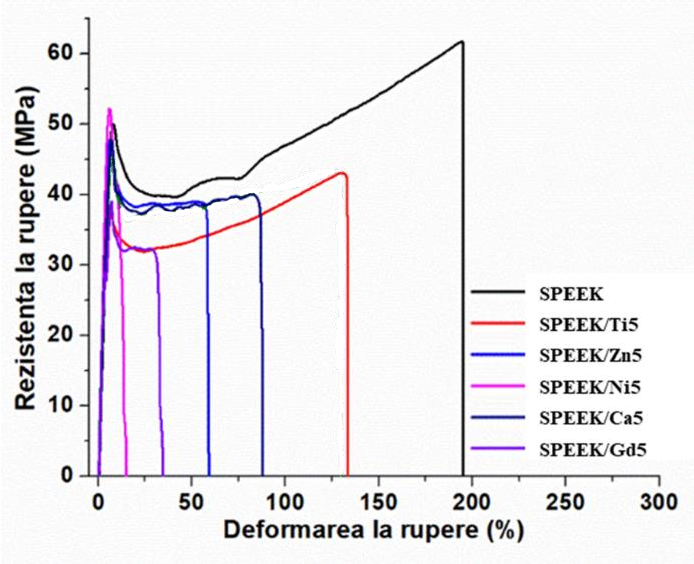

Figure 4.7. Tensile strain-stress curves

Proton conductivity is a key parameter, being directly proportional to the power output of a fuel cell [40]. The performance of the composite membranes was evaluated using broadband dielectric spectroscopy under an alternating electric field with an applied voltage of 1 V. The conductivity was calculated using the following equation:

$$\sigma = \omega \varepsilon'' \varepsilon_0 \quad (17)$$

Proton conductivity effects are typically manifested by a conductivity plateau in the low-frequency region. This plateau can be attributed to membrane polarization arising from the presence of free charge carriers (in this case, protons) and dipolar species (sulfonic acid groups). At higher frequencies, the time interval between successive reversals of the electric field becomes too short for the free charge carriers (protons) to migrate to the membrane–electrode interface, resulting in the appearance of a second conductivity plateau. In this high-frequency region, interfacial phenomena occurring at the electrode-membrane interface or between membrane components have a reduced influence on the measured response. Therefore, proton conductivity is estimated from the conductivity plateau observed at high frequencies.

The conductivity values measured at high frequencies are presented in Table 4.6. For all membranes, a decrease in conductivity is observed at temperatures above 40-60 °C. This reduction is attributed to water evaporation from the membrane, which adversely affects proton transport. For membranes containing 5 wt.% filler, with thicknesses ranging from 40 to 70 μm and measured under an applied voltage of 1 V, conductivity values lower than those of the reference SPEEK membrane were obtained, with the exception of the membrane containing titanium dioxide. Furthermore, all membranes, including the reference SPEEK membrane, exhibited lower conductivity values than the commercial reference membrane (Nafion), tested under identical conditions. Nevertheless, among the composite membranes, the best performance was achieved by those containing praseodymium doped zinc ferrite and nickel ferrite particles, together with the membrane incorporating titanium dioxide, which was included as a benchmark filler for comparison.

Table 4.6. Hydrated membranes conductivity at 10^7 Hz and different temperatures

Sample	Conductivity (S/cm)					
	20 °C	**40 °C**	**60 °C**	**80 °C**	**100 °C**	**120 °C**
SPEEK	1,2E-03	1,5E-03	1,5E-04	5,4E-06	7,0E-07	2,4E-07
SPEEK/Ti5	1,0E-03	1,5E-03	6,6E-04	3,6E-05	3,2E-06	6,2E-07
SPEEK/Zn5	4,0E-04	4,0E-04	6,4E-05	3,3E-06	4,3E-07	1,6E-07
SPEEK/Ni5	2,7E-04	2,8E-04	3,8E-05	7,4E-07	2,0E-07	1,0E-07
SPEEK/Ca5	1,7E-05	2,0E-05	5,6E-06	5,6E-07	2,1E-07	1,3E-07
SPEEK/Gd5	2,2E-05	1,3E-05	1,1E-06	1,7E-07	9,3E-08	7,1E-08
Nafion117	3,8E-03	3,4E-03	2,4E-03	1,4E-03	6,9E-04	4,0E-04

4.3. The effect of filler content variation

As mentioned in the previous chapter, two metal oxides ($ZnFe_{1,96}Pr_{0,04}O_4$ and $NiFe_{1,96}Pr_{0,04}O_4$) were selected for a detailed investigation of the effect of filler loading on the properties of the composite membranes. In this section, a comprehensive characterization of the composite membranes was carried out, including the determination of ion exchange capacity (IEC), water uptake (WU) at 80 °C, and proton conductivity using Nyquist plot analysis. The experiments were performed on membranes with thicknesses ranging from 150 to 180 μm, which were characterized under an alternating voltage of 10 mV. Under these experimental conditions, the SPEEK/TiO_2 membranes exhibited conductivity values similar to or lower than those of the pristine SPEEK membrane.

4.3.1. SPEEK/$ZnFe_{1,96}Pr_{0,04}O_4$ composite membranes

To investigate the effect of the $ZnFe_{1,96}Pr_{0,04}O_4$ filler on the properties of the composite membranes, a series of membranes containing different filler loadings was prepared. Four composite membranes were fabricated using the filler concentrations presented in Table 4.8.

Table 4.8. IEC, WU and filler content of SPEEK/$ZnFe_{1,96}Pr_{0,04}O_4$ composite membranes

Sample	Filler content (%)	IEC	WU% (RT)	WU% (80 °C)
SPEEK	0	1,71	24	44,2
SPEEK/Zn0.25	0,25	1,67	24,5	40,2
SPEEK/Zn1	1	1,69	25,3	41,6
SPEEK/Zn3	3	1,78	25,8	32,1
SPEEK/Zn5	5	1,80	26,3	32,6

The morphology of the membranes containing different amounts of praseodymium-doped zinc ferrite was evaluated by SEM (Figure 4.10). Careful examination of the micrographs indicates that the composite membranes possess a dense structure, free of pores and cracks. Furthermore, the SEM images recorded from the cross-sections of the samples, obtained by fracturing the membranes in liquid nitrogen, reveal that the filler is homogeneously distributed throughout the membrane bulk.

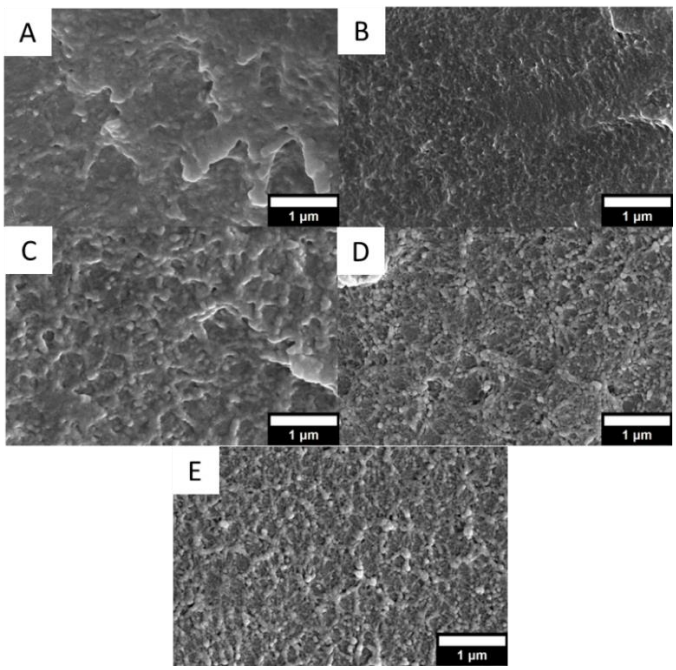

Figure 4.10. SEM images of; A- SPEEK; B- SPEEK/Zn0.25; C- SPEEK/Zn1; D- SPEEK/Zn3; D- SPEEK/Zn5

For proton-conducting membranes, water plays an indispensable role and is essential for both the performance and proper operation of PEMFC [8]. The ion exchange capacity (IEC), water uptake (WU), and proton conductivity of polymer membranes are closely interrelated. Within the membrane structure, water is associated with the acid functional groups, forming hydrophilic domains and channels that connect the two surfaces of the membrane. These channels facilitate proton transport across the membrane. However, beyond a certain level, excessive water uptake can adversely affect the mechanical stability of the membrane, leading to reduced performance [128,129].

The ion exchange capacity and water uptake values are presented in Table 4.8. Based on the obtained ion exchange capacity values, it can be concluded that the filler does not block or isolate the acidic functional groups within the membrane. On the contrary, the presence of the filler contributes positively to the ion exchange capacity, which shows a slight increase with increasing filler content.

The water uptake values measured at room temperature are very similar to that of the pristine membrane, ranging from 24.0% for the SPEEK membrane to 26.3% for the membrane containing 5% praseodymium doped zinc ferrite. At 80 °C, water uptake decreases for all composite membranes compared to the pristine SPEEK membrane. However, this decrease does not vary linearly with filler content. The reduction amounts to only a few percentage points for membranes containing low filler loadings (0.25 and 1%), whereas a more pronounced decrease, exceeding ten percentage points, is observed for membranes containing higher filler loadings (3 and 5%).

The incorporation of the filler does not compromise the thermal stability, chemical stability, or mechanical properties of the membranes, confirming their suitability as PEM.

Proton conductivity is considered one of the most important performance parameters of PEMFC membranes. There are two principal mechanisms responsible for proton transport through a hydrated membrane [41]. The mechanism generally regarded as having the greatest contribution to proton transport is the Grotthuss mechanism, also known as the proton hopping mechanism. In this process, protons are transferred between neighboring proton-conducting sites through a network of hydrogen bonds. The second mechanism is the vehicular mechanism, in which protons associate with water molecules (the solvent) to form complex ionic species, such as H_3O^+, these species subsequently diffuse through the membrane [172].

The results obtained by dielectric spectroscopy were evaluated for validity, linearity, and stability using the Kramers–Kronig test [23]. The analysis was performed using the AfterMath software package, version 1.6.10523 [187] (Figure 4.15).

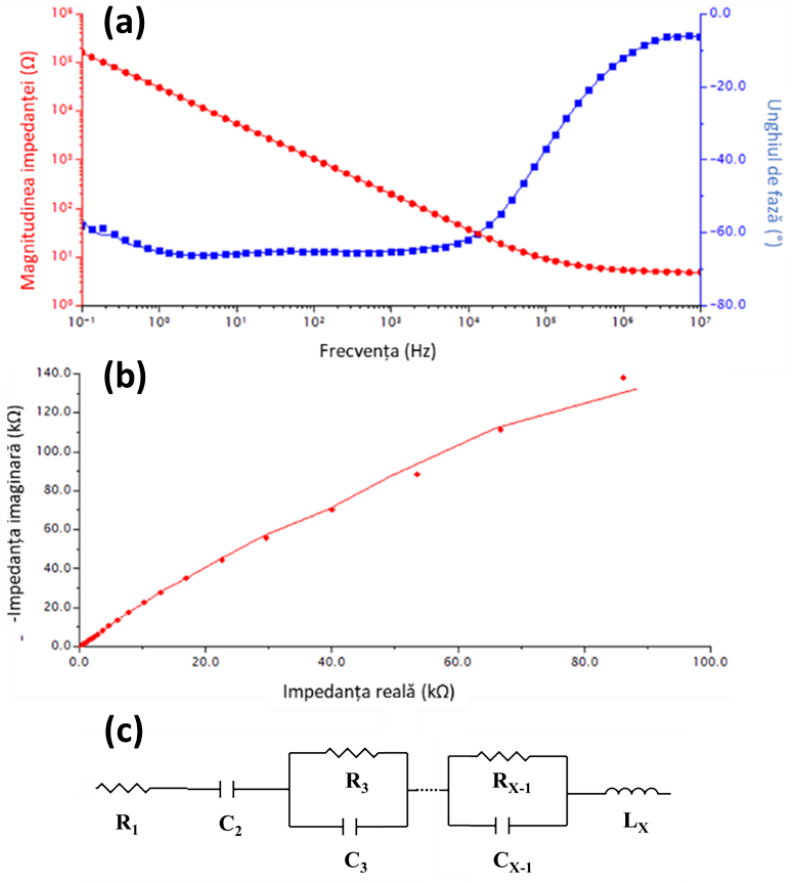

Figure 4.15. Kramers–Kronig test for the data obtained for the SPEEK membrane at 20 °C: (a) Bode plot, (b) Nyquist plot, and (c) equivalent circuit model employed by the software for fitting the experimental data.

Figure 4.16a shows the frequency dependence of the dielectric constant (ε`) for the SPEEK and SPEEK/$ZnFe_{1,96}Pr_{0,04}O_4$ membranes containing different filler concentrations, and Nafion117. The decrease in dielectric constant with increasing frequency can be attributed to ionic polarization effects resulting from proton migration through the membrane, as well as the orientation of dipolar species. Among the investigated membranes, SPEEK/Zn0.25 exhibits the highest dielectric constant values at high frequencies. This behavior indicates a greater degree of polarization arising from mobile ions and dipoles, which is reflected in its higher proton conductivity (Table 4.12).

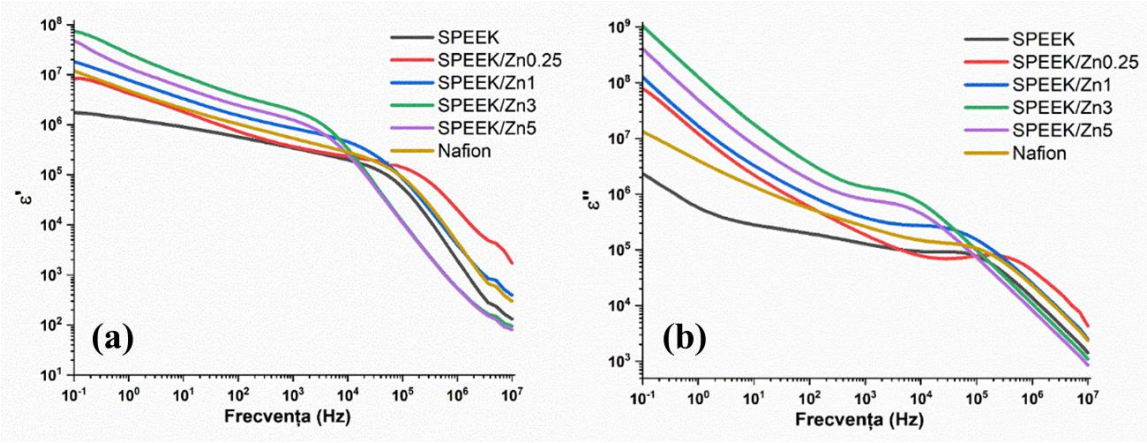

Figura 4.16. Frequency dependence of the dielectric constant (a) and dielectric loss (b) for the pristine SPEEK membrane, SPEEK/$ZnFe_{1,96}Pr_{0,04}O_4$ composite membranes, and Nafion117

Figure 4.16b presents the dielectric loss of the composite membranes. The dielectric loss decreases with increasing frequency. At low frequencies, the measured dielectric loss values can be attributed to electrode polarization, resulting from the accumulation of free charges at the electrode-membrane interface, as well as to Maxwell-Wagner-Sillars (MWS) polarization, which is particularly characteristic of composite membranes containing higher filler loadings. The dielectric constant and dielectric loss values at low frequencies ($\leq 10^4$ Hz) increase with increasing filler content up to a loading of 3%, while lower values are observed for the SPEEK/Zn5 membrane. The reduced values obtained for the membrane containing 5% filler may be attributed to ferrite particle agglomeration and the consequent reduction in polymer chain mobility. In addition, membrane polarization may become localized around agglomerated filler within the membrane, resulting in a decrease in the overall dielectric constant.

At high frequencies ($\geq 10^5$ Hz), the dielectric constant exhibits a steeper decline because the applied electric field alternates more rapidly, preventing dipoles and mobile charge carriers from reorienting at a rate comparable to the field variation, as a consequence, the dielectric loss decreases. The ohmic behavior of the membranes can be examined within this frequency range, since dipoles rarely align with the externally applied electric field at high frequencies and macroscopic polarization effects become negligible [92]. The shoulder observed in the intermediate-frequency region may be attributed to the macroscopic polarization of ionic charge carriers. The frequency at which the slope changes in the logarithmic representation of the dielectric constant versus frequency, as well as the inflection point in the dielectric loss versus frequency plot, shifts as a function of filler content. For the SPEEK/Zn0.25 membrane, both the slope change and the dielectric loss

inflection point occur at higher frequencies (Figure 4.16). As the concentration of praseodymium doped zinc ferrite increases, the transition shift toward lower frequencies.

Based on the measured water uptake and ion exchange capacity values, it can be concluded that the number of free charge carriers in the composite membranes does not change significantly with increasing filler content. Considering the processes occurring within the membranes during the dielectric measurements, it can be inferred that low filler loadings enhance ion mobility, whereas higher concentrations of praseodymium doped zinc ferrite (3 and 5%) lead to a reduction in ion mobility. The improvement in ion mobility at low filler concentrations may be attributed to enhanced connectivity between hydrophilic domains and the formation of well-connected proton conducting pathways. The increase in dielectric constant observed at low frequencies is associated with electrode polarization, which is present in all membranes, as well as Maxwell-Wagner-Sillars (MWS) polarization, which occurs in the composite membranes [188].

In the Nyquist plots (Figure 4.19), the ohmic resistance is typically associated with the high frequency intercept of the semicircle on the real axis. Both the charge-transfer resistance and the double layer capacitance contribute to the depressed semicircle observed in the intermediate frequency region. At low frequencies, a straight line is generally observed, corresponding to the diffusion process of ionic species, which in the present case are protons. The proton conductivity of the composite membrane can be calculated from the membrane resistance determined from the low-frequency intercept of this line on the real axis. The proton conductivity, σ (S cm^{-1}), was calculated using the following equation:

$$\sigma = L/(R_b \times S) \quad (18)$$

where L is the membrane thickness (cm), R_b is the membrane resistance obtained from the high-frequency intercept with the X axis in the Nyquist plot, and S is the electrode area.

The proton conductivity values obtained at different temperatures for the hydrated pristine SPEEK membrane, the SPEEK/Znx composite membranes, and Nafion, used as a reference, are presented in Table 4.12. As expected, the proton conductivity increases with temperature for all samples up to approximately 60 °C. At higher temperatures, membrane dehydration leads to a decrease in proton conductivity for all tested membranes. The SPEEK/Zn0.25 and SPEEK/Zn1 composite membranes exhibit higher proton conductivity than the pristine SPEEK membrane. This improvement in conductivity can be attributed to several factors.

The presence of the $ZnFe_{1,96}Pr_{0.04}O_4$ filler may contribute to a more uniform distribution of the acidic groups responsible for the formation of hydrophilic domains and hydrogen-bonding networks, thereby promoting proton conductivity. The good compatibility between the praseodymium-doped zinc ferrite, $ZnFe_{1,96}Pr_{0,04}O_4$, and the SPEEK polymer matrix may improve phase connectivity, leading to the formation of hydrophilic channels that are more favorable for proton transport through the membrane. However, as the filler content increases, a decrease in proton conductivity is observed. This reduction may be related to inadequate dispersion or aggregation of $ZnFe_{1,96}Pr_{0.04}O_4$ particles, which hinders the formation of continuous hydrophilic channels and limits proton transport.

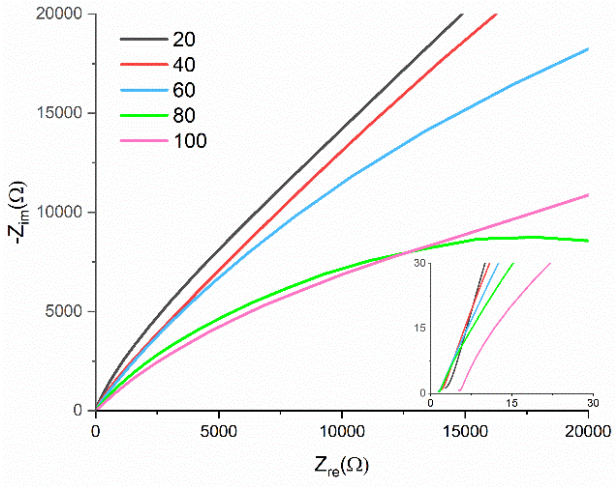

Figure 4.19. Nyquist plot for SPEEK/Zn0.25 at different temperatures

Table 4.12. Proton conductivity of SPEEK/$ZnFe_{1,96}Pr_{0,04}O_4$ composite membranes

Proba	**Conductivity ×10^{-2} S/cm**				
	20 °C	**40 °C**	**60 °C**	**80 °C**	**100 °C**
SPEEK	0,43	0,64	0,83	0,81	0,63
SPEEK/Zn0.25	1,44	2,75	3,41	2,82	2,25
SPEEK/Zn1	0,50	1,04	1,57	1,26	0,82
SPEEK/Zn3	0,21	0,49	0,62	0,47	0,24
SPEEK/Zn5	0,14	0,29	0,47	0,21	0,02
Nafion117	1,36	1,56	1,60	1,26	0,73

4.3.2. SPEEK/$NiFe_{1,96}Pr_{0,04}O_4$ composite membranes

In addition to the composite membranes containing $ZnFe_{1,96}Pr_{0,04}O_4$, a series of composite membranes incorporating $NiFe_{1,96}Pr_{0,04}O_4$ was also prepared by varying the content of praseodymium doped nickel ferrite. The doped nickel ferrite was synthesized using the same procedure employed for the preparation of the doped zinc ferrite. Three composite membranes were fabricated, containing 1, 3 and 5% filler.

Table 4.13. IEC, WU and filler content of SPEEK/$NiFe_{1,96}Pr_{0,04}O_4$ composite membranes

Membrane	Filler content (%)	IEC	WU% (RT)	WU% (80 °C)
SPEEK	0	1,71	24,0	44,2
SPEEK/Ni1	1	1,84	24,2	47,1
SPEEK/Ni3	3	1,87	24,2	36,7
SPEEK/Ni5	5	1,61	25,2	36,3

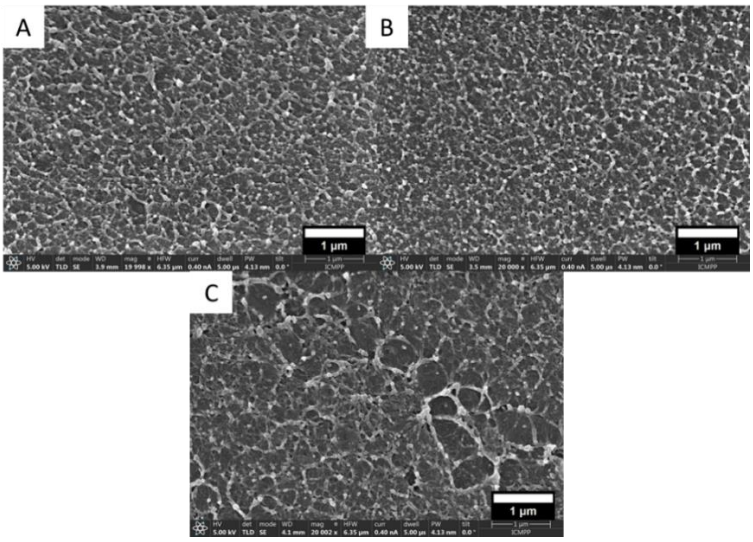

Figure 4.21. SEM images of A- SPEEK/Ni1; B- SPEEK/Ni3 and C- SPEEK/Ni5

The SPEEK/$NiFe_{1,96}Pr_{0.04}O_4$ composite membranes obtained (Figure 4.21) are dense and free of pores or cracks. The praseodymium doped nickel ferrite is well dispersed throughout the membrane matrix, although a slight tendency toward agglomeration can be observed, most likely due to its magnetic properties. Nanoparticle agglomeration is already noticeable at relatively low filler loadings, starting at 1% $NiFe_{1,96}Pr_{0.04}O_4$. This behavior is most likely associated with the higher magnetization of nickel ferrite compared to zinc ferrite.

At room temperature, the water uptake values of the composite membranes are similar to that of the pristine SPEEK membrane, being 24.0% for SPEEK and 24.2% for both SPEEK/Ni1 and SPEEK/Ni3. The only exception is the membrane containing 5 wt.% filler, which exhibits a slightly higher water uptake of 25.2%. Water sorption measurements performed at 80 °C (Figure 4.22b) show an increase in water uptake for the SPEEK/Ni1 membrane, reaching 47.1%, compared with 44.2% for the pristine SPEEK membrane. However, this improvement is not maintained with increasing filler content, as the water uptake decreases for the SPEEK/Ni3 and SPEEK/Ni5 membranes.

As in the case of the membranes containing praseodymium doped zinc ferrite, the incorporation of praseodymium doped nickel ferrite does not compromise the thermal stability, chemical stability, or mechanical properties of the membranes, confirming their suitability for PEMFC applications.

The phenomena responsible for the decrease in these parameters are the same as those discussed in the previous case. However, a difference between the SPEEK/$NiFe_{1,96}Pr_{0.04}O_4$ membranes and the SPEEK/$ZnFe_{1,96}Pr_{0.04}O_4$ membranes is observed in the dielectric constant. The nickel ferrite-containing membranes exhibit lower dielectric constant values at low frequencies than both the pristine SPEEK membrane and Nafion117. This behavior may be explained by the tendency of the praseodymium doped nickel ferrite particles to agglomerate. Furthermore, domains may exist within the membrane in which polarization at the ferrite-polymer exists, leading to a reduction in the overall dielectric response of the membrane.

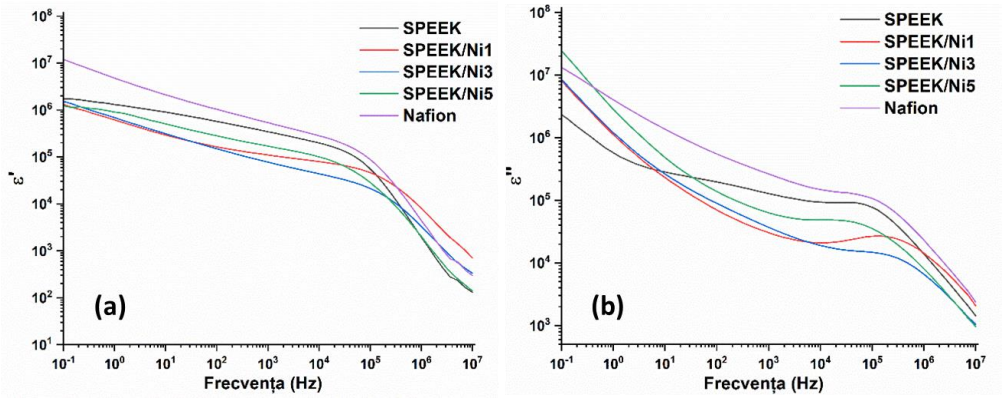

Figure 4.25. Frequency dependence of the dielectric constant (a) and dielectric loss (b) for the pristine SPEEK membrane, SPEEK/$NiFe_{1,96}Pr_{0,04}O_4$ composite membranes, and Nafion117

The proton conductivity values determined from the Nyquist plots are presented in Table 4.17. Proton conductivity increases for the membrane containing 1 % praseodymium

doped nickel ferrite and subsequently decreases with increasing filler content. As observed for the SPEEK/$ZnFe_{1,96}Pr_{0.04}O_4$ membranes, the decrease in proton conductivity at higher filler loadings may be associated with poor dispersion or aggregation of the $NiFe_{1,96}Pr_{0.04}O_4$, particles, which hinders the formation of continuous hydrophilic channels and limits both proton transport and Maxwell-Wagner-Sillars (MWS) polarization. The highest proton conductivity value was obtained for the SPEEK/Ni1 membrane at 80 °C, reaching 1.72×10^{-2} S/cm. This value exceeds the highest conductivity measured for Nafion117, which was $11,6\times10^{-2}$ S/cm at 60 °C.

Table 4.17. Proton conductivity of SPEEK/$NiFe_{1,96}Pr_{0,04}O_4$ composite membranes

Sample	Conductivity $\times10^{-2}$ S/cm				
	20 °C	40 °C	60 °C	80 °C	100 °C
SPEEK	0,43	0,64	0,83	0,81	0,63
SPEEK/Ni1	0,43	0,85	1,25	1,72	0,72
SPEEK/Ni3	0,29	0,46	0,56	0,61	0,01
SPEEK/Ni5	0,26	0,37	0,55	0,42	0,02
Nafion	1,36	1,56	1,60	1,26	0,73

4.4. Proton conductivity of the composite membranes containing core@shell nanoparticles

To investigate the effect of $ZnFe_{1,96}Pr_{0,04}O_4@TiO_2$ and $NiFe_{1,96}Pr_{0,04}O_4@TiO_2$ nanoparticles on the SPEEK matrix, a series of composite membranes containing different filler loadings was prepared. The proton conductivity values obtained for representative composite membranes are presented in Table 4.18. The best performance was achieved for the SPEEK/$ZnFe_{1,96}Pr_{0,04}O_4@TiO_2$ membrane containing 1 wt.% filler, which exhibited a proton conductivity of $3,26\times10^{-2}$ S/cm at 60 °C. This conductivity is comparable to that obtained for the SPEEK/$ZnFe_{1,96}Pr_{0,04}O_4$ membranes, for which the maximum value of $3,41\times10^{-2}$ S/cm was recorded for the membrane containing 0.25 % filler at 60 °C.

Table 4.18. Proton conductivity of composite membranes

Sample	Conductivity $\times10^{-2}$ S/cm				
	20 °C	40 °C	60 °C	80 °C	100 °C
SPEEK/Zn@Ti0,5	1,04	1,33	1,62	1,50	1,19
SPEEK/Zn@Ti1	1,46	2,68	3,26	2,92	1,76

SPEEK/Zn@Ti3	0,68	1,02	1,35	1,24	0,37
SPEEK/Ni@Ti1	0,57	0,77	1,15	1,09	0,13
SPEEK/Ni@Ti3	0,42	0,79	1,47	1,35	0,47

4.5. Performance analysis based of polarization curves

The SPEEK/Zn0.1 membrane was successfully tested in a single fuel cell system. The polarization curve obtained for the SPEEK/Zn0.1 membrane is presented in Figure 4.27.

The maximum power density achieved by the composite membrane was 91 mW/cm^2. The open circuit voltage (OCV) of the fuel cell was 0.96 V, a value typical for SPEEK-based membranes, which are known to exhibit low gas crossover (undesired gas permeation or diffusion through the membrane) [95].

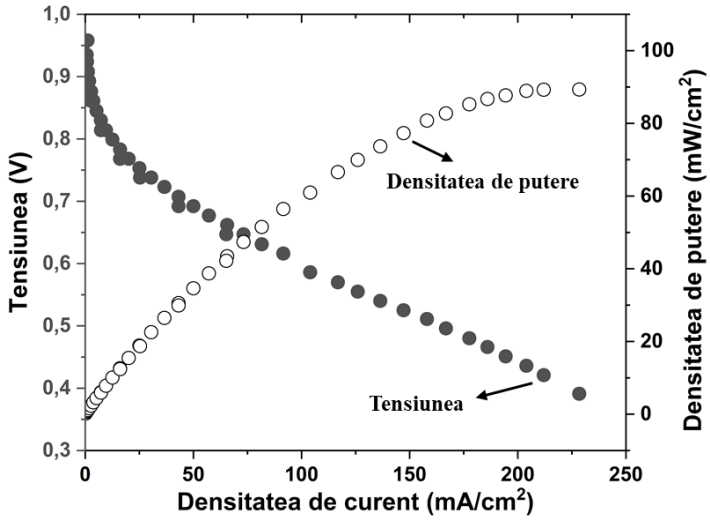

Figure 4.27. Polarization curve for SPEEK/Zn0.1 membrane

4.6. Conclusions

Seven SPEEK-based composite membranes containing 5% filler were prepared using TiO_2, $CaMnO_3$, Gd_2MnFeO_6, $CoFe_2O_4$, $ZnFe_{1,96}Pr_{0,04}O_4$, $NiFe_{1,96}Pr_{0,04}O_4$ or $Zn_{0,5}Ni_{0,5}Fe_{1,96}Pr_{0,04}O_4$ as filler materials. Following a comparative evaluation of the obtained results, $ZnFe_{1,96}Pr_{0,04}O_4$ and $NiFe_{1,96}Pr_{0,04}O_4$ were selected for further investigation in order to assess the effect of filler loading on the properties of the composite membranes. Considering the requirements for application in proton exchange membrane fuel cells, the following membrane properties were evaluated: ion exchange capacity, water uptake, thermal stability, mechanical properties, chemical stability, membrane morphology, and proton conductivity.

The proton conductivity of the composite membranes was determined using broadband dielectric spectroscopy. The highest conductivity values were obtained for the membrane containing 1% $ZnFe_{1,96}Pr_{0,04}O_4@TiO_2$ $3{,}26\times10^{-2}$ S/cm, and for the membrane containing 3% $NiFe_{1,96}Pr_{0,04}O_4@TiO_2$ $1{,}47\times10^{-2}$ S/cm °C, both measured at 60 °C. The SPEEK/Zn0.1 membrane was successfully tested in a single fuel cell system, achieving a maximum power density of 91 mW/cm^2.

5. GENERAL CONCLUSIONS

This doctoral thesis is part of the ongoing efforts to develop decarbonization strategies through the use of proton exchange membrane fuel cells, with a focus on the polymer electrolyte membrane. The work is dedicated to the study of novel proton exchange membrane systems capable of achieving or even surpassing the performance of commercially available PFSA-based PEM.

The thesis is structured around two main specific objectives: (i) the synthesis and characterization of novel metal oxides, and (ii) the demonstration of the feasibility of the use of these oxide materials as fillers in composite membrane systems.

The metal oxides intended for use as fillers in the composite membranes four ferrites (**$CoFe_2O_4$**, **$ZnFe_{1,96}Pr_{0,04}O_4$**, **$NiFe_{1,96}Pr_{0,04}O_4$** and **$Zn_{0,5}Ni_{0,5}Fe_{1,96}Pr_{0,04}O_4$)** and two perovskites (**$CaMnO_3$** and **Gd_2MnFeO_6**) were synthesized by a modified sol-gel auto-combustion method. Metal nitrates were used as cation precursors, with the exception of gadolinium (Gd_2O_3). The combustion agents were selected based on synthesis: citric acid and ethylene glycol for the perovskites, anthranilic acid used for the first time in the synthesis of cobalt ferrite and urea for the praseodymium doped ferrites. Structural characterization confirmed the successful formation of the desired phases.

Furthermore, the ferrites that exhibited the best performance in the composite membranes were transformed into core@shell nanoparticles, through the polycondensation of TTIP in the presence of the ferrite particles, using citric acid as a surfactant.

The magnetic properties, evaluated from room-temperature hysteresis curves, revealed negligible magnetization for $CaMnO_3$ (<1 emu/g), low values for Gd_2MnFeO_6 și $ZnFe_{1,96}Pr_{0,04}O_4$ (≈ 4 emu/g), intermediate values for $NiFe_{1,96}Pr_{0,04}O_4$ (31 emu/g), and high magnetization values for $CoFe_2O_4$ and $Zn_{0,5}Ni_{0,5}Fe_{1,96}Pr_{0,04}O_4$ (69 and 62 emu/g, respectively). TEM analysis revealed irregularly shaped nanoparticles with average particle sizes of 220 nm for $CaMnO_3$ and Gd_2MnFeO_6, 81 nm for $CoFe_2O_4$, 23 nm for both $ZnFe_{1,96}Pr_{0,04}O_4$ și $NiFe_{1,96}Pr_{0,04}O_4$, and 29 nm for $Zn_{0,5}Ni_{0,5}Fe_{1,96}Pr_{0,04}O_4$.

To achieve the second objective, (*iia*) the sulfonation method of poly(ether ether ketone) (PEEK) was optimized through the application of ultrasonic irradiation, resulting in a significant reduction in synthesis time and precise control of the degree of sulfonation, a parameter that directly influences the performance of SPEEK; and (*iib*) the synthesized metal oxides, obtained as nano- and submicron-sized particles, were evaluated as fillers capable of enhancing the proton conductivity of the SPEEK matrix. The properties of the

resulting membranes, including morphology, water uptake capacity, chemical and thermal stability, mechanical properties, and proton conductivity, were investigated for two classes of composite membranes. Thin membranes with thicknesses ranging from 40 to 70 μm, containing 5% filler and characterized by broadband dielectric spectroscopy under an applied voltage of 1 V, generally exhibited lower performance than the pristine SPEEK matrix. The poorest results were obtained for the membranes containing perovskite fillers, while the SPEEK/Ti5 showing a slight improved performance relative to the pristine membrane.

A detailed investigation was carried out by dielectric spectroscopy at an applied voltage of 10 mV on composite membranes containing varying amounts of filler, namely SPEEK/$ZnFe_{1,96}Pr_{0,04}O_4$, SPEEK/$NiFe_{1,96}Pr_{0,04}O_4$ SPEEK/$ZnFe_{1,96}Pr_{0,04}O_4$@TiO_2 and SPEEK/$NiFe_{1,96}Pr_{0,04}O_4$@TiO_2. The investigated membranes had thicknesses ranging from 150 to 180 μm.

Under these experimental conditions, the **SPEEK/Zn0.25** membrane exhibited a proton conductivity of (**3,41×10^{-2} S/cm at 60°C**), significantly exceeding the pristine SPEEK membrane (**SPEEK**, **0,83×10^{-2} S/cm at 60°C**) and Nafion117 (**1,60×10^{-2} S/cm at 60°C**), which were used as reference materials. The best performance for praseodymium doped nickel ferrite membranes was achieved by the **SPEEK/Ni1 1,72×10^{-2} S/cm at 80°C**, for the core@shell composite membranes, the one containing **1% $ZnFe_{1,96}Pr_{0,04}O_4$@TiO_2 (3,26×10^{-2} S/cm at 60°C),** and **3% $NiFe_{1,96}Pr_{0,04}O_4$@TiO_2 (1,47×10^{-2} S/cm at 60 °C)**. The SPEEK/Zn0.1 membrane was further evaluated in a single-cell fuel cell configuration, achieving a maximum power density of 91 mW cm^{-2}, thereby demonstrating the potential applicability for PEMFC operation.

The studies carried out on SPEEK-based composite membranes containing oxide fillers with different structures, morphologies, and compositions provided a detailed understanding of the factors influencing the physicochemical properties of the membranes. Furthermore, they enabled the identification of membrane systems that satisfy the requirements for application in proton exchange membrane fuel cells (PEMFC), exhibiting proton conductivity values comparable to or even exceeding those of the commercially available Nafion membrane.

The results obtained during the course of this doctoral research benefited from partial financial support provided through a national research project. Led to the filing of a patent application, published in two scientific papers, and presented at three scientific conferences.

REFERENCES

8. Mauritz, K.A.; Moore, R.B. State of Understanding of Nafion. *Chemical Reviews* **2004**, *104*, 4535–4585, doi:10.1021/cr0207123.

15. Huang, R.Y.M.; Shao, P.; Burns, C.M.; Feng, X. Sulfonation of Poly(Ether Ether Ketone)(PEEK): Kinetic Study and Characterization. *Journal of Applied Polymer Science* **2001**, *82*, 2651–2660, doi:10.1002/app.2118.

23. Weiß, A.; Schindler, S.; Galbiati, S.; Danzer, M.A.; Zeis, R. Distribution of Relaxation Times Analysis of High-Temperature PEM Fuel Cell Impedance Spectra. *Electrochimica Acta* **2017**, *230*, 391–398, doi:10.1016/j.electacta.2017.02.011.

40. Wilkinson, D.P.; Zhang, J.; Hui, R.; Fergus, J.; Li, X. *Proton Exchange Membrane Fuel Cells : Materials Properties and Performance*; CRC Press: Boca Raton, 2009; ISBN 9781439806647.

41. Kreuer, K.D. On the Development of Proton Conducting Polymer Membranes for Hydrogen and Methanol Fuel Cells. *Journal of Membrane Science* **2001**, *185*, 29–39, doi:10.1016/S0376-7388(00)00632-3.

92. Samoila, P.; Grecu, I.; Asandulesa, M.; Cojocaru, C.; Harabagiu, V. Bio-Based Ionically Cross-Linked Alginate Composites for PEMFC Potential Applications. *Reactive and Functional Polymers* **2021**, *165*, 104967, doi:10.1016/j.reactfunctpolym.2021.104967.

95. Raja, K.; Raja Pugalenthi, M.; Ramesh Prabhu, M. The Effect of Incorporation of Ferrous Titanate Nanoparticles in Sulfonated Poly(Ether Ether Ketone)/Poly (Amide Imide) Acid-Base Polymer for Cations Exchange Membrane Fuel Cells. *Journal of Solid State Electrochemistry* **2020**, *24*, 35–44, doi:10.1007/s10008-019-04453-9.

115. Jian-hua, T.; Peng-fei, G.; Zhi-yuan, Z.; Wen-hui, L.; Zhong-qiang, S. Preparation and Performance Evaluation of a Nafion-TiO2 Composite Membrane for PEMFCs. *International Journal of Hydrogen Energy* **2008**, *33*, 5686–5690, doi:10.1016/j.ijhydene.2008.07.036.

121. Kreuer, K.D.; Paddison, S.J.; Spohr, E.; Schuster, M. Transport in Proton Conductors for Fuel-Cell Applications: Simulations, Elementary Reactions, and Phenomenology. *Chemical Reviews* **2004**, *104*, 4637–4678, doi:10.1021/cr020715f.

128. Barjola, A.; Reyes-Rodríguez, J.L.; Solorza-Feria, O.; Giménez, E.; Compañ, V. Novel SPEEK-ZIF-67 Proton Exchange Nanocomposite Membrane for PEMFC Application at Intermediate Temperatures. *Industrial and Engineering Chemistry Research* **2021**, *60*, 9107–9118, doi:10.1021/acs.iecr.1c01780.

129. Martina, P.; Gayathri, R.; Pugalenthi, M.R.; Cao, G.; Liu, C.; Prabhu, M.R. Nanosulfonated Silica Incorporated SPEEK/SPVdF-HFP Polymer Blend Membrane for PEM Fuel Cell Application. *Ionics* **2020**, *26*, 3447–3458, doi:10.1007/s11581-020-03478-9.

152. Kundu, S.; Akanksha; Sheetal; Thakur, S.; Kumar, V.; Pani, B.; Singh, M.; Singh, A.K. A Critical Review on Nano Ferrites Pioneering a Paradigm Shift in Corrosion Inhibition towards Different Metal/Alloys in Diverse Corrosive Environments. *Journal of Environmental Chemical Engineering* **2025**, *13*, 115277, doi:10.1016/j.jece.2024.115277.

153. Mansour, H.; Okba, E.A.; Ibrahim, M.M.; Elshami, F.I.; Shaban, S.Y. A Kinetic and Mechanistic Study of Chitosan-Functionalized Lanthanum Zinc Ferrite Nanoparticles: Balancing Biomolecular Affinity with Anticancer, Antibacterial, and Antioxidant Functions. *Inorganic Chemistry Communications* **2025**, *181*, 115230, doi:10.1016/j.inoche.2025.115230.

154. Ahmad, W.; Shah, R.; Khan, J.A.; Shah, N.S.; Al-Anazi, A.; Alelyani, S.S.; Kavil, Y.N.; Castro-Muñoz, R.; Boczkaj, G. TiO_2 and Non-Metal Doped TiO_2 Nanoparticles: Synthesis and Applications for Green Energy Production. *International Journal of Hydrogen Energy* **2025**, *149*, 150024, doi:10.1016/j.ijhydene.2025.06.214.

155. Wang, T.; Qian, X.; Yue, D.; Yan, X.; Yamashita, H.; Zhao, Y. CaMnO3 Perovskite Nanocrystals for Efficient Peroxydisulfate Activation. *Chemical Engineering Journal* **2020**, *398*, 125638, doi:10.1016/j.cej.2020.125638.

156. Sivasamy, R.; Venugopal, P.; Espinoza-González, R. Structure, Electronic Structure, Optical and Magnetic Studies of Double Perovskite Gd_2MnFeO_6 Nanoparticles: First Principle and Experimental Studies. *Materials Today Communications* **2020**, *25*, doi:10.1016/j.mtcomm.2020.101603.

164. Spurr, R.A.; Myers, H. Quantitative Analysis of Anatase-Rutile Mixtures with an X-Ray Diffractometer. *Analytical Chemistry* **1957**, *29*, 760–762, doi:10.1021/ac60125a006.

166. Zhong, Y.; Zhang, X.; Xia, Y.; Zhang, L.; Xu, Q.; Zhu, X.; Feng, W.; Qin, Q. A Fresh Perspective on the Impact of $ZnTiO_3$ Coupling on the Microstructure and Photocatalytic Properties of TiO_2 Fabricated at Varied Temperatures. *Molecules* **2023**, *28*, 7626, doi:10.3390/molecules28227626.

167. Pang, S.; Huang, J. guo; Su, Y.; Geng, B.; Lei, S. yuan; Huang, Y. ting; Lyu, C.; Liu, X. juan Synthesis and Modification of Zn-Doped TiO_2 Nanoparticles for the Photocatalytic Degradation of Tetracycline. *Photochemistry and Photobiology* **2016**, *92*, 651–657, doi:10.1111/PHP.12626.

168. Naseri, M.G.; Saion, E.B.; Hashim, M.; Shaari, A.H.; Ahangar, H.A. Synthesis and Characterization of Zinc Ferrite Nanoparticles by a Thermal Treatment Method. *Solid State Communications* **2011**, *151*, 1031–1035, doi:10.1016/j.ssc.2011.04.018.

169. Samoila, P.; Baltag, L.; Cojocaru, C.; Ignat, M.; Harabagiu, V. Quick Process for Poly(Aryl-Ether)Ketone Sulphonation 2021, RO134943A2.

170. Baltag, L.; Cojocaru, C.; Enache, A.C.; Samoila, P.; Harabagiu, V. Ultrasonic-Assisted Rapid Preparation of Sulfonated Polyether Ether Ketone (PEEK) and Its Testing in Adsorption of Cationic Species from Aqueous Solutions. *Materials* **2022**, *15*, 7558, doi:10.3390/ma15217558.

172. Raja Pugalenthi, M.; Punyawudho, K.; Anbu Arasi, M.; Shah, A.A.; Ramesh Prabhu, M.; Kouthaman, M.; Velsankar, K.; Gayathri, R. Designing High Performance Electrospuned SPEEK Nanofibers Composite Membrane for PEMFC Application. *Materials Letters* **2023**, *339*, 134117, doi:10.1016/j.matlet.2023.134117.

179. Islam, A.; Shahriar, M.; Islam, M.T.; Teo, S.H.; Khan, M.A.R.; Taufiq-Yap, Y.H.; Mohanta, S.C.; Rehan, A.I.; Rasee, A.I.; Kubra, K.T.; Hasan, M.M.; Salman, M.S.; Waliullah, R.M.; Hasan, M.N.; Sheikh, M.C.; Uchida, T.; Awual, M.E.; Hossain, M.S.; Znad, H.; Awual, M.R. Advances in Filler-Crosslinked Membranes for Hydrogen Fuel Cells in Sustainable Energy Generation. *International Journal of Hydrogen Energy* **2025**, *140*, 745–776, doi:10.1016/j.ijhydene.2025.05.197.

187. AfterMath Electrochemical Studio 1.6.10523 | Pine Research Instrumentation: https://pineresearch.com/downloads/aftermath-1-6-10523/.

188. Samet, M.; Levchenko, V.; Boiteux, G.; Seytre, G.; Kallel, A.; Serghei, A. Electrode Polarization vs. Maxwell-Wagner-Sillars Interfacial Polarization in Dielectric Spectra of Materials: Characteristic Frequencies and Scaling Laws. *Journal of Chemical Physics* **2015**, *142*, doi:10.1063/1.4919877.